ARTICLE TEMPLATE

# Analytical predictor-corrector entry guidance for hypersonic gliding vehicles

Huatao Chen[a], Kun Zhao [b], Juan LG Guirao[c], Dengqing Cao[d]

[a] Division of Dynamics and Control, School of Mathematics and Statistics, Shandong University of Technology, Zibo 255000, China
[b] Beijing Electro-mechanical Engineering Institute, Beijing 100074, China
[c] Departamento de Matemática Aplicaday Estadística, Universidad Politécnica de Cartagena, 30203-Cartagena, Spain
[d] Division of Dynamics and Control, School of Astronautics, Harbin Institute of Technology, Harbin 150001, China

**ABSTRACT**
For the entry guidance problem of hypersonic gliding vehicles, an analytical predictor-corrector guidance method based on feedback control of bank angle is proposed. First, the relative functions between the velocity, bank angle and range-to-go are deduced, and then, the analytical relation is introduced into the predictor-corrector algorithm, which is used to replace the traditional method to predict the range-to-go via numerical integration. To eliminate the phugoid trajectory oscillation, a method for adding the aerodynamic load feedback into the control loop of the bank angle is proposed. According to the quasi-equilibrium gliding condition, the function of the quasi-equilibrium glide load along with the velocity variation is derived. For each guidance period, the deviation between the real time load and the quasi-equilibrium gliding load is revised to obtain a smooth reentry trajectory. The simulation results indicate that the guidance algorithm can adapt to the mission requirements of different downranges, and it also has the ability to guide the vehicle to carry out a large range of lateral maneuvers. The feedback control law of the bank angle effectively eliminates the phugoid trajectory oscillation and guides the vehicle to complete a smooth reentry flight. The Monte Carlo test indicated that the guidance precision and robustness are good.

**KEYWORDS**
Entry guidance, Analytical predictor corrector, Hypersonic gliding vehicle, Quasi-equilibrium glide, Feedback control.

## 1. Introduction

Generally, a hypersonic gliding vehicle (HGV) refers to an aircraft adapted in the near space for long distance gliding that uses a lift-body configuration and a no-power gliding flight mode, and typically, its flight Mach number is much than 5. Compared with the traditional ballistic reentry vehicle, an HGV has many advantages, such as a fast remote arrival, a strong maneuvering capability, a flexible and changeable trajectory, and a large area coverage [1]. Entry guidance in aerospace engineering refers to the

Email: htchencn@sdut.edu.cn(HC);kunzhaohit@yeah.net(KZ);juan.garcia@upct.es(JLG);dqcao@hit.edu.cn(DC)

onboard process in which the steering commands for an HGV with an aerodynamic lifting capability are generated, so as to guide the vehicle from its initial condition to safely and accurately reach the specified final condition [2]. For the reentry process of these vehicles, the range of altitude and velocity is very large, and strict constraints in the heating rate, dynamic pressure and load factor, as well as the high sensitivity to the control variables for the hypersonic reentry trajectory, create challenges. The entry guidance algorithm mainly includes: reference trajectory entry guidance and predictor corrector entry guidance [3]. Reference trajectory guidance is a method to track the nominal trajectory of prebinding in the onboard computer by designing a control algorithm. Reference trajectory guidance has the advantages of limited calculations, a simple guidance system and minimal requirements for the onboard computer, but the disadvantage is that the landing accuracy is greatly affected by deviations from the initial entry states and entry environmental disturbances. Thus, it is difficult to meet the needs of long-range precision attack [4, 5]. Multiple Model Tracking for HGV with Aerodynamic Modeling and Analysis have been considered by Li et al[6]

Predictor corrector entry guidance was first proposed by Anderson, Schultz,and Stolarik [7], and this algorithm for real-time correction of the guidance command predicts the landing position. It can significantly reduce the effect of the initial dispersion error on the guidance performance, and it also is very robust against various entry errors [8]. For the enhanced predictor corrector Mars entry guidance approach with atmospheric uncertainties, one can refer to [9]. Lu proposed predictor corrector entry guidance based on the Newton-Raphson method for different lift-to-drags (L/D) of hypersonic vehicles [2]. The longitudinal and lateral motion are separated by a quasi-equilibrium glide condition (QEGC), and a guidance law was correspondingly designed. The longitudinal guidance computed the size of bank angle via a numerical integration of the ballistic equations to predict the range-to-go in combination with an iterative correction algorithm. In the lateral control is the use of bank angle reversal logic or lateral reference trajectory tracking for guidance [10, 11]. Based on fuzzy logic, Wang, Zhang, and Tang [12] considered predictor-corrector guidance for entry vehicle .Brunner compared the performance of a numerical predictor corrector (NPC) skip entry guidance algorithm with that of the Apollo skip entry guidance. NPC algorithms are highly adaptive, especially in the face of extreme dispersion and off-nominal situations. The class of predictor-corrector algorithms has evolved and emerged to have great potential. One of the keys to predictor-corrector algorithms is how to accurately and rapidly predict the range-to-go. An NPC predicts the range-to-go of the vehicle via numerical integration of ballistic equations [13]. The main advantage of an NPC is that it can address any possible flight conditions and can predict the landing point, load and heating rate in advance; thus, it has a strong ability to adapt. Due to the requirements for fast prediction, there are strict requirements for the performance of the on-board computer. An analytical predictor corrector (APC) finds an approximate analytical solution from all or part of the trajectory to predict the range-to-go. This method avoids the numerical integration of ballistic equations, thus significantly reducing the number of calculations and time required [14]. An APC is suitable for online operation of the on-board computer due to its simplicity, but a weakness of this algorithm has been the lack of effective means to enforce inequality trajec-tory constrains such as those on the heating rate and aerodynamic load. Some researchers have proposed a method to solve this problem by adding an altitude rate feedback in the closed loop guidance [2, 13]. To shape the altitude profile for improved trajectory characteristics and enforcement of inequality trajectory constraints, the entry guidance algorithm design not entirely dependent on the QEGC, and the guidance algorithm must be

modified to eliminate the phugoid trajectory oscillation.

In this paper, based on the QEGC, a high accuracy analytical solution was obtained for predicting the range-to-go, and it was introduced into the predictor-corrector algorithm. In fact, the essence of the phugoid trajectory oscillation is that the normal aerodynamic load can not always follow the quasi-equilibrium glide load, which causes a periodic variation in the altitude in the longitudinal plane. By analyzing the trajectory characteristics of an HGV, the quasi-equilibrium glide load was obtained. Then, we proposed a closed loop guidance algorithm based on the feedback of the aerodynamic load. In the following content, we will verify that this method is also very effective.

## 2. Preliminary

### 2.1. Entry Dynamics

For the high lift-to-drag ratio vehicles with low orbital velocities investigated in this paper, the Coriolis inertial force and centrifugal inertial force caused by the earths self rotation are small, compared with the aerodynamic force and gravity. Therefore, the nonrotating spherical earth assumption is employed in the analytical guidance law design [19]. The three degree-of-freedom (3DOF) point-mass dynamics of a vehicle over a non-rotating spherical rotating earth are adopted:

$$\dot{r} = v \sin \gamma, \tag{1}$$

$$\dot{\theta} = \frac{v \cos \gamma \sin \psi}{r \cos \phi}, \tag{2}$$

$$\dot{\phi} = \frac{v \cos \gamma \sin \psi}{r}, \tag{3}$$

$$\dot{v} = -D - \frac{\sin \gamma}{r^2}, \tag{4}$$

$$\dot{\gamma} = \frac{1}{v} \left[ L \cos \sigma + \left( v^2 - \frac{1}{r} \right) \frac{\cos \gamma}{r} \right], \tag{5}$$

$$\dot{\psi} = \frac{1}{v} \left[ \frac{L \sin \sigma}{\cos \gamma} + \frac{v^2}{r} \cos \gamma \sin \psi \tan \phi \right], \tag{6}$$

where $r$ is the radial distance from the earths center to the vehicle normalized by the equatorial radius of the Earth, $R_0 = 6378.135m$. The longitude and latitude are $\theta$ and $\phi$, respectively. Earths relative velocity $v$ is normalized by $v_{scale} = \sqrt{g_0 R_0}$ with $g_0 = 9.81m/s^2$. The relative flight path angle is $\gamma$, and $\sigma$ is the bank angle. The relative velocity azimuth angle $\psi$ is measured clockwise in the local horizontal plane from the north. The differentiation is with respect to the dimensionless time $\tau = \frac{t}{\sqrt{\frac{R_0}{g_0}}}$.

Finally, terms $L$ and $D$ represent the nondimensional aerodynamic lift and drag acceleration in $g_0$, respectively,

$$\begin{cases} L = K \rho v^2 C_L \\ D = K \rho v^2 C_D \end{cases}$$

where $K = \frac{R_0 S}{2m}$, and $S$ is the vehicle reference area. $C_L(\alpha, M)$ and $C_D(\alpha, M)$ are the lift and drag coefficients as functions of the angle of attack $\alpha$ and Mach number $M$. The vehicle mass $m$ is normalized by the initial mass $m_0$. $\rho$ is the atmospheric density,

and it is expressed as an exponential model:

$$\rho = \rho_0 e^{-\beta R_0 (r-1)}$$

where $\rho_0$ is the density at sea level and $\beta$ is a constant.

## 2.2. Entry Path Constraints

To avoid compromising the structural integrity of the vehicle, the operational boundaries must be determined by considering the heating rate, dynamic pressure, and aerodynamic load. The constraints include the following:

$$
\begin{aligned}
Q &= K_Q \sqrt{\rho} v^{3.15} \leq Q_{\max} \\
q &= 0.5 \rho v^2 R_0 g_0 \leq q_{\max} \\
n &= \sqrt{L^2 + D^2} \leq n_{\max}
\end{aligned}
$$

where $K_Q = k_s \times \left(\sqrt{g_0 R_0}\right)^{3.15}$ for the constant $k_s$. The values of $Q_{\max}, q_{\max}$ and $n_{\max}$ are all specified. All of the preceding three constraints are considered "hard" constraints because they should be observed with a reasonably tight tolerance.

The lower operating boundaries for the heating rate, dynamic pressure and aerodynamic load in the $h - v$ plane are

$$h > \max\left\{ -\frac{2}{\beta} \ln\left(\frac{Q_{\max}}{k_Q \sqrt{\rho} v^{3.15}}\right), -\frac{1}{\beta} \ln\left(\frac{2q_{\max}}{\rho_0 v^2 R_0 g_0}\right), -\frac{1}{\beta} \ln\left(\frac{n_{\max}}{K \rho_0 v^2 \sqrt{L^2 + D^2}}\right) \right\}.$$

The variation rule of the maximum atmospheric density $\rho_{\max}$ with velocity based on the $h - v$ plane can be obtained, and then, the change rule for the maximum lift $L_{\max}$ with the velocity $v$ can be obtained using the lift formula.

Consider the equilibrium glide condition, which is obtained by setting $\dot{\gamma}$ in Eq. (5):

$$L \cos\sigma - \left(\frac{1}{r^2} - \frac{v^2}{r}\right) \frac{\cos\gamma}{r} = 0. \tag{7}$$

Set $\sigma = \sigma_{QEGC}$, and approximate $r \approx 1$ and $\gamma \approx 0$. The result can be called the QEGC $L \cos\sigma + (v^2 - 1) = 0$. The QEGC can be used to calculate the maximum bank angle boundary $\sigma_{QEGC\,\max} = \arccos\frac{1-v^2}{L_{\max}}$. For vehicles with medium or higher $\frac{L}{D}$, another possible path constraint is $L \cos\sigma_{EQ} + (v^2 - 1) \leq 0$, where $\sigma_{EQ}$ is the specified bank angle. This constraint can help to reduce the phugoid oscillations in the altitudes along the entry trajectory, and preserve a sufficient bank angle margin that accounts for trajectory dispersions. This constraint is a soft constraint, and violation of the constraint would not pose a safety risk or endanger the mission success. According to the above treatment, the path constraint change for the bank angle constraint follows

$$\sigma_{EQ} \leq \sigma \leq \sigma_{QEGC\,\max}. \tag{8}$$

## 2.3. Entry Terminal Constraints

Without loss of generality, an energy-like variable $e$ , will be used as the independent variable for guidance algorithm development

$$e = \frac{1}{r} - \frac{v^2}{2} \tag{9}$$

As the typical terminal constraints, the trajectory reaches a position at a specified distance $s_f$, from the target site at a specified final altitude $r_f$ , and velocity $v_f$ . Thus,

$$\begin{cases} r(\tau_f) = r_f^*, \\ v(\tau_f) = v_f^*, \\ s(\tau_f) = s_f^* \end{cases} \tag{10}$$

where $s$ denotes the great-circle range to the landing site, which is normalized by $R_0$ (hence, $s$ is in radians), and it is a function of the longitude and latitude.

## 3. Analytical Predictor-Corrector Guidance Algorithm

Similar to the conventional gliding guidance method, the gliding guidance is still divided into two part: longitudinal guidance and lateral guidance. The difference is that this paper uses an analytical prediction method for the longitudinal guidance. The lateral guidance is used to determine the sign of the bank angle to meet the requirements of the lateral deviation of the terminal.

### 3.1. Longitudinal guidance law design

The reentry trajectory begins at an altitude where the aerodynamic forces are quite small. Therefore, open loop guidance is adopted in this section. The constant bank angle $\sigma_0$ is selected as the control variable in this stage, and its symbol is

$$sign(\sigma_0) = -sign(\Delta\psi). \tag{11}$$

The current heading offset is defined as $\Delta\psi = \psi - \psi_{LOS}$, where $\psi_{LOS}$ is the azimuth angle at the current location along the great circle connecting the current location and the target location and $\psi_{LOS}$ is the current actual azimuth angle. In the process of flight, the altitude oscillation amplitude usually appears after the first trough. An altitude rate $\dot{h}$, equal to zero for the first time is selected as the hand-off time between the initial descending segment and the gliding segment.

#### 3.1.1. Equilibrium glide solution

Suppose that the flight path angle is small in the process of gliding [15]; then, according to Eq.(7), the relationship between the velocity and altitude can be obtained as

$$v = \frac{1}{r} \left( \frac{C_L S_\rho R_0 \cos\sigma}{2m} + \frac{1}{r} \right)^{-\frac{1}{2}}. \tag{12}$$

5

The atmospheric density of the gliding process can also be obtained,

$$\rho = \frac{2m\cos\gamma}{SC_L v^2 R_0 \cos\sigma}\left(\frac{1}{r^2} - \frac{v^2}{r}\right). \tag{13}$$

Differentiating by $v$ on both sides of Eq.(13),

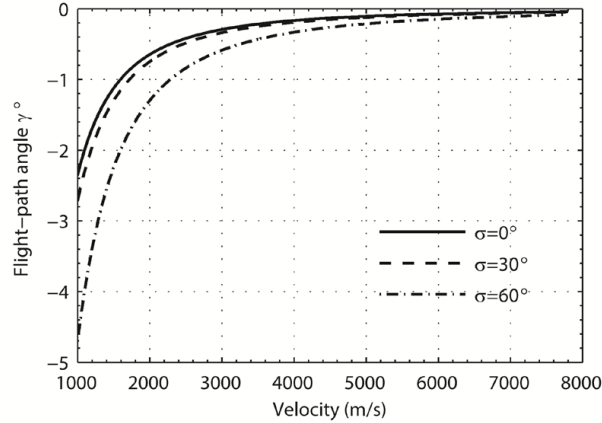$$\frac{d\rho}{dv} = -\frac{4m\cos\gamma}{SC_L v^3 r^2 R_0 \cos\sigma}. \tag{14}$$

Using the atmospheric density index model from Eqs.(4) and (7), we obtain

$$\frac{dv}{d\rho} = \frac{D}{\rho\beta v R_0 \sin\gamma} + \frac{1}{\rho\beta v r^2 R_0}. \tag{15}$$

By contrast Eqs.(14) and (15), the relationship between the flight path angle and the velocity was obtained using the QEGC,

$$\tan\gamma = -\frac{1}{K^*\cos\sigma\left[0.5\beta r^2 v^2 R_0 + (1 - v^2 r)^{-1}\right]} \tag{16}$$

where $K^* = \frac{L}{D}$ is the lift-to-drag ratio. Eqs.(13) and (16) form the approximate solution when the vehicle is gliding, which is the function of the velocity.



**Figure 1.** Curve of the flight path angle as a function of the velocity.

Figure 1 illustrates the flight path angle with the velocity curves at different bank angles. The flight path angle gradually increased with a decrease in the velocity, and the greater the bank angle is, the greater the flight path angle. When the bank angle is less than 60 degrees, the maximum flight path angle is less than 5 degrees, which indicates that the small angle assumption of flight path angle is accurate.

Both sides of Eq.(7) were divided by the lift-to-drag ratio $K^*$, we resulting in

$$D = \frac{\cos\gamma}{K^*\cos\sigma}\left(\frac{1}{r^2} - \frac{v^2}{r}\right). \tag{17}$$

We substitute Eq.(17) into Eq.(4); according to the small angle assumption for the flight path angle, $\cos\gamma \approx 1$ and $\sin\gamma \approx 0$, we obtain

$$\frac{dv}{v^2 r - 1} = \frac{d\tau}{r^2 K^* \cos\sigma}. \tag{18}$$

Since to is a small amount in the reentry process, it could be approximated that $r \approx 1$. By setting the initial time $\tau_0 = 0$ on both sides of Eq.(18), and integrating, we obtain

$$\ln\left|\frac{v(\tau) - 1}{v(\tau) + 1}\right| - \ln\left|\frac{v_0 - 1}{v_0 + 1}\right| = \frac{2\tau}{K^* \cos\sigma}. \tag{19}$$

In general, $0 < v(\tau) < 1$, we let

$$\lambda(\tau) = \frac{2\tau}{K^* \cos\sigma} + \ln\left|\frac{v_0 - 1}{v_0 + 1}\right|, \tag{20}$$

and by substituting Eq.(20) into Eq.(19), we obtain the velocity expression about time

$$v(\tau) = \frac{1 - e^{\lambda(\tau)}}{1 + e^{\lambda(\tau)}}. \tag{21}$$

According to Eqs.(1),(7) and (14), we obtain the altitude expression about velocity

$$h = \frac{2}{\beta}\left(\ln\frac{v}{v_0} + \frac{1}{2}\ln\frac{1 - v_0^2}{1 - v^2}\right) + h_0 \tag{22}$$

where $h_0$ is the initial altitude.

The actual range-to-go is defined as a large arc that connects the current position to the target position, which is calculated as

$$S_{togo} = \cos^{-1}\left[\sin\phi\sin\phi_f + \cos\phi\cos\phi_f\cos(\theta_f - \theta)\right], \tag{23}$$
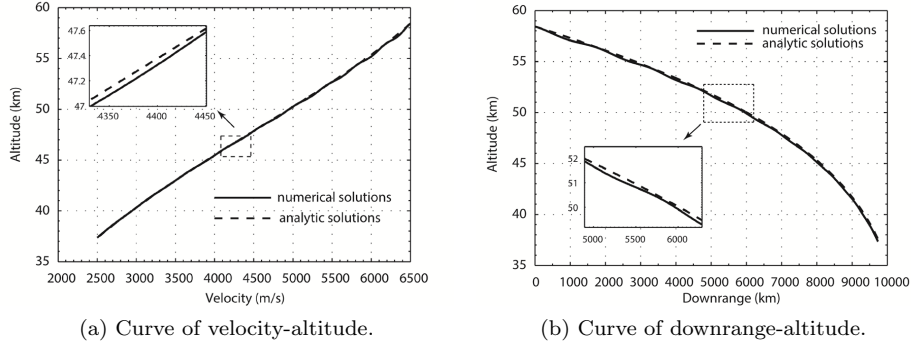
where $\theta_f$ and $\phi_f$ are the latitude and longitude at the target position, respectively. When the offset between the azimuth of this great circle and the azimuth angle $\Delta\psi$ is ignored, the differential equation for predicted the range-to-go $s_p$ is [13, 16]

$$\dot{s}_p = \frac{ds}{d\tau} = -\frac{v}{r}\cos\gamma. \tag{24}$$

By contrasting Eqs.(18) and (24), the relationship between velocity and predicted range-to-go can be obtained after integration. Thus,

$$s_p = \frac{1}{2}K^* \cos\sigma \ln\frac{rv^2 - 1}{rv_0^2 - 1}. \tag{25}$$

Taking CAV-H as an example, the lift-to-drag ratio is $K^*$, the initial velocity is $v_0 = 6500m/s$ , and the end condition is $v_f = 2500m/s$ . Using Eqs.(12) and (16), we obtain the corresponding equilibrium glide altitude and flight path angle are 58.45km and $-0.0632^o$, respectively. The equilibrium glide solution is taken as the initial value

(a) Curve of velocity-altitude.     (b) Curve of downrange-altitude.

**Figure 2.** Comparison between the analytical solution and numerical solution.

of the dynamic equations (1)–(6), and then the dynamic equations are numerically solved. The comparison between the analytical solution and the numerical solution is shown in Figure 2. The calculation results show that the downrange deviation is 0.6868% and the altitude deviation is 0.7232%, which indicates that the numerical solution has sufficient accuracy.

For the purpose of entry guidance, the gliding distance of the terminal should satisfy

$$s_f(\sigma) = s_{togo} - s_p = s_{togo} - \frac{1}{2}K^* \cos\sigma \ln\frac{rv_f^2 - 1}{rv_0^2 - 1} = 0. \tag{26}$$

Since the terminal gliding distance is a nonlinear function of the bank angle , we can use the secant method to ad-just the size of the bank angle,

$$|\sigma_{i+1}| = |\sigma_i| - \frac{|\sigma_i| - |\sigma_{i-1}|}{s_{f,i} - s_{f,i-1}} s_{f,i}. \tag{27}$$

For each guidance period, when Eq.(26) is satisfied, the value of the bank angle $\sigma_{base}$ is taken as a longitudinal guidance command, and the symbol of the bank angle is decided by the lateral guidance logic.

### 3.1.2. Feedback control law design

Without relying on QEGC constraints, the guidance command $\sigma_{base}$ is unable to guide the vehicle to complete a smooth reentry flight. By constantly adjusting the bank angle, the aerodynamic load also changes in the longitu-dinal plane, which is one of the reasons for the oscillation of the reentry trajectory. One design idea for the longitudinal guidance includes adding a feedback control in the outer loop of the bank angle to eliminate the phugoid trajectory oscillation. The calculation formula is

$$|\sigma_{cmd}| = |\sigma_{base} - k(n_N - n_{ref}), \tag{28}$$

where $n_N$ is the real-time normal aerodynamic load, $n_{ref}$ is the reference load, and $k > 0$ is the gain. A phugoid trajectory oscillation means that the normal aerodynamic load cannot always follow the quasi-equilibrium glide load, which causes a periodic variation in the altitude in the longitudinal plane.

It is known that the dynamic pressure formula is $q = 0.5\rho v^2 g_0 R_0$, and in differential

form, we have

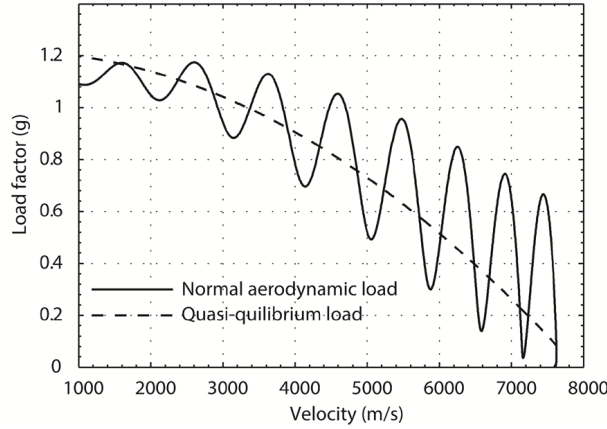$$\frac{dq}{dv} = \frac{1}{2}g_0 R_0 \left( \frac{d\rho}{dv}v^2 + \rho v \right). \tag{29}$$

Substituting Eq.(14) into Eq.(29) and integrating with respect to $v$, we obtain

$$q = \frac{mg_0 \cos\gamma}{C_L S \cos\sigma} \left( \frac{1}{r^2} - \frac{v^2}{r} \right). \tag{30}$$

Eq.(30) is substituted into the definition of a normal aerodynamic load, $n_N = L\cos\alpha + D\sin\alpha$ , to obtain the quasi-equilibrium glide load,

$$n_{QEGC} = \frac{1 + K^{*-2}}{\cos\sigma} \left( \frac{1}{r^2} - \frac{v^2}{r} \right). \tag{31}$$

The different types of entry vehicles also have different quasi-equilibrium glide loads. There are three main types of entry vehicles. The first is a capsule crew exploration vehicle (CEV), and its hypersonic trim $\frac{L}{D}$ ratio is approximately 0.28. The second vehicle is the X-33, which has a medium hypersonic $\frac{L}{D}$ ratio of approximately 0.9. The third vehicle model is a generic high performance Common Aero Vehicle, called a CAV. The CAV has a high maximum $\frac{L}{D}$ ratio of 3.5 at hypersonic speeds [2]. The quasi-equilibrium glide load required for the CEV is the largest, followed by X-33, and it is the smallest for the CAV.



**Figure 3.** Curves of load factor versus velocity.

The quasi-equilibrium glide load is a monotonically decreasing function of the velocity (Figure 3). Generally the initial entry state of a hypersonic glide vehicle is not satisfied by the QEGC, which will cause the normal aerodynamic load to fluctuate near the quasi-equilibrium load, and this ultimately leads to the creation of a skip gliding trajectory. In addition, when an HGV performs an entry mission, the bank angle can be adjusted at any time according to the guidance directive, which is bound to aggravate the degree of oscillation.

To eliminate the phugoid trajectory oscillation and guide the vehicle to complete

the smooth reentry flight, let $n_{ref} = n_{QEGC}$ ; then, Eq. (38) becomes

$$|\sigma_{cmd}| = |\sigma_{base}| - k(n_N - n_{QEGC}) \tag{32}$$

During each guidance period, the deviation between the real-time normal aerodynamic load and the quasi equilibrium glide load is revised to obtain a smooth reentry trajectory. Typically, the trajectory is pulled up too high after the initial dive and then continues to oscillate for the rest of the trajectory. Therefore, during the early stage of reentry, the feedback control law of the bank angle should focus on eliminating the periodic oscillation, and it should select the larger gain. During the later stage of reentry, the feedback control law should focus on the correction of the downrange and select the smaller gain. The gain, $k > 0$, may be scheduled as a linear function of the velocity, and a piecewise decreasing function is used to represent the gain coefficient

$$k = \begin{cases} k_1, & v > v_1, \\ k_2, & v_2 < v \le v_1, \\ 0, & v \le v_2 \end{cases} \tag{33}$$

where $k_1$ and $k_2$ are set according to the actual reentry initial state and terminal constraints.

### 3.1.3. Lateral guidance law design

The lateral motion of an entry vehicle is controlled by the sign of its bank angle, as determined by the entry guidance system [11]. The conventional technique for changing the bank angle sign is based on prespecified threshold values in the azimuth error of the vehicle with respect to the target site. A lateral threshold based on the crossrange and range-to-go is proposed to determine the sign of the bank angle command and control the terminal heading error [23]. It has been confirmed that this method is more effective than the azimuth error for lateral guidance, and this paper also adopts this lateral guidance method.
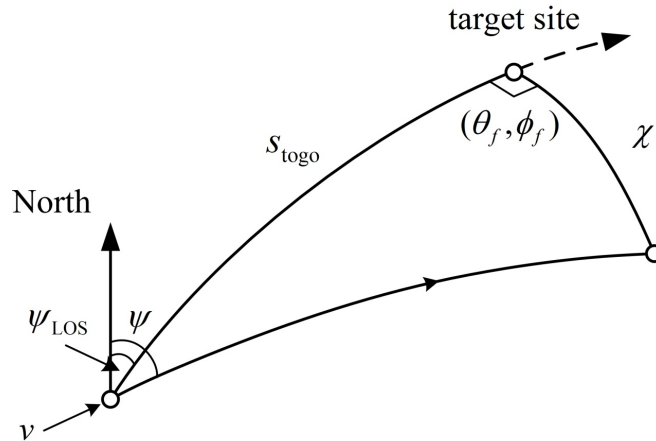


**Figure 4.** Spherical geometry of the crossrange.

The crossrange at the target site is $\chi$, as shown in Figure 4. The formula for calcu-

10

lating the crossrange is

$$\chi = -\sin^{-1}\left[\sin s_{togo}\sin(\psi - \psi_{LOS})\right], \qquad (34)$$
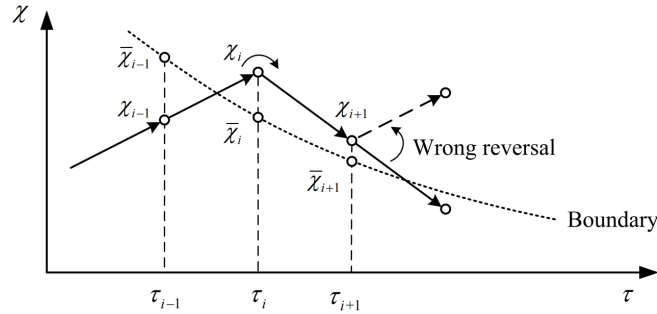
where the range-to-go $s_{togo}$ and $\psi_{LOS}$ are the same as defined in section 3.1. Figure 4 illustrates the spherical triangle by which relationship Eq. (44) is derived. The formula for calculating the azimuth angle is

$$\psi_{LOS} = -sin^{-1}\left(\frac{\sin(\theta_f - \theta)\cos\phi_f}{\sin s_{togo}}\right). \qquad (35)$$

Define the crossrange reference boundary as

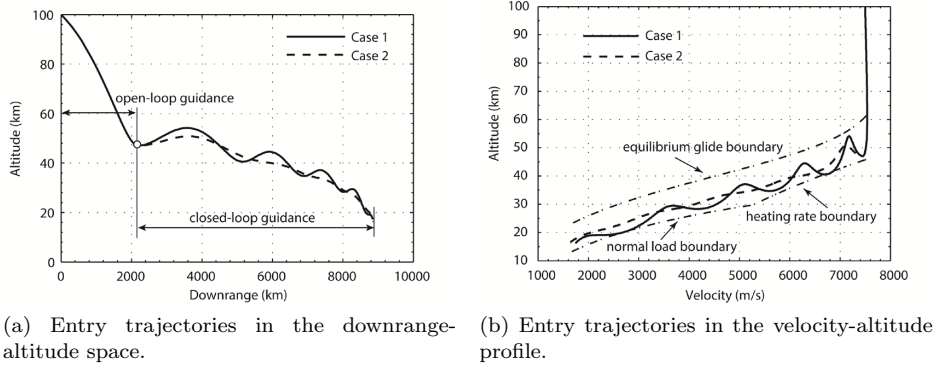$$\overline{\chi} = -\sin\left(\sin s_{togo}\sin(\Delta\psi)\right), \qquad (36)$$

where $\Delta_{ref} = \frac{(\Delta\psi_0 - \Delta\psi_f)s_{togo}}{s} + \Delta\psi_f$ is the reference azimuth angle deviation and $\Delta\psi_0, \Delta\psi_f$ are representa-tive of the initial and terminal azimuth angle deviations, respectively. and determine the beginning and end of the opening size of the crossrange boundary, respectively. To realize control of the lateral trajectory, it is necessary to find a suitable reversal logic for the bank angle. The basic principle of reversal logic is to design a symmetric reference crossrange boundary with the downrange as the center. When the vehicle reaches the reference crossrange boundary, the bank angle sign switched, and the motion of the vehicle is reversed, which ensures that the vehicle is always in the interior of the reference crossrange boundary.



**Figure 5.** A special case of lateral reversal logic.

This study found that in one case the reversal logic will fail, as shown in Figure 5. Assuming that the crossrange $\chi_i$ during the $i$-th guidance period is more than the lateral boundary threshold $\overline{\chi}_i$, the sign of the bank angle is reversed; During the $(i + 1)$-th guidance period, the crossrange $\chi_{i+1}$ is still more than the current lateral boundary threshold $\overline{\chi}_{i+1}$, and the bank angle will still be reversed according to the reversal logic. At this time, the reversal logic is wrong, which will cause the vehicle to glide in a direction away from the lateral boundary. As a result, the lateral error becomes increasingly, which leads to the failure of the guidance algorithm. To avoid a guidance logic error, a novel lateral guidance logic is designed, that is,

$$S_\sigma(\tau_i) = \begin{cases} sgn(\sigma(\tau_{i-1}), |\chi_i| \le \overline{|\chi_i|}, \\ sgn(S_\sigma(\tau_{i-1})), |\chi_i| \ge |\overline{\chi}_i| \& |\chi_{i-1}| > |\overline{\chi}_{i-1}|, \\ -sgn(S_\sigma(\tau_{i-1})), |\chi_i| \ge |\overline{\chi}_i| \& |\chi_{i-1}| < |\overline{\chi}_{i-1}|. \end{cases} \qquad (37)$$

11

(a) Entry trajectories in the downrange-altitude space.

(b) Entry trajectories in the velocity-altitude profile.

**Figure 6.** Trajectory characteristics for the longitudinal plane.

Combined with the magnitude of the bank angle that was determined, the final guidance law for the bank angle is

$$\sigma_{cmd} = S_{sigma}|\sigma_{cmd}|. \tag{38}$$

## 4. Simulation analysis

The CAV-H vehicle model is used in the numerical computation in this section. Its main characteristic parameters include a weight $m$, of approximately 907.2kg and a reference area of $0.4839m^2$. The path constraints in the entry gliding include a maximum heating rate of $Q_{\max} = 800kW/m^2$, a maximum dynamic pressure of $q_{\max} = 300kPa$ and a maximum load factor of $n_{\max} = 5.0g$. The following nominal angle of the attack profile $\alpha$ is used for all cases

$$\alpha = \begin{cases} 45deg, & if M \geq 10, \\ 45 - 0.612(M - 10)^2 deg, & if 2.5 \leq M \leq 10. \end{cases} \tag{39}$$
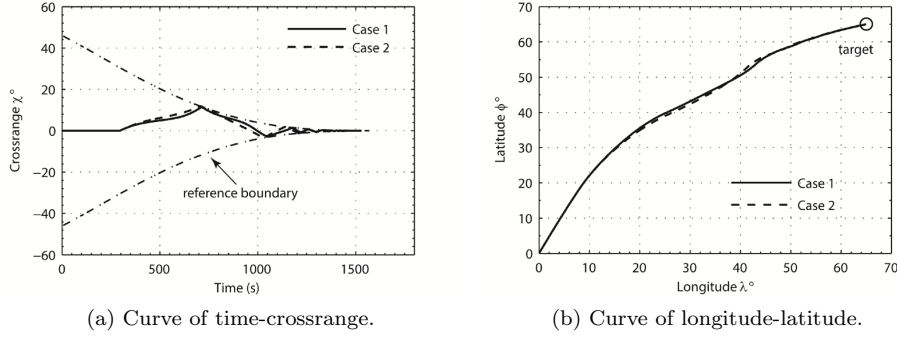
where $M$ is the Mach number.

### 4.1. Typical trajectory simulation

As the first step, we wanted to verify the validity of the analytical predictor-corrector guidance algorithm and then compare the effects of applying a feedback bank angle control to the trajectory. In the following simulation, we designed two cases: (1) only using the analytical predictor-corrector guidance algorithm and (2) applying the analytical predictor-corrector guidance algorithm with the feedback bank angle control (Eq.(33)).

The initial reentry state of the vehicle was set to an initial altitude of $h_0 = 100$ km, a velocity of $v_0 = 7500m/s$, initial latitude and longitude coordinates of $(0°, 0°)$ , a flight-path angle of $\gamma_0 = -0.8°$, an azimuth angle of $\psi_0 = -22.90°$ . We set the initial azimuth angle deviation $\Delta\psi_0 = 30°$, and the terminal azimuth angle deviation $\Delta\psi_f = 0°$ . Terminal constraints included: a target site of $(E65°, N65°)$, a terminal altitude of $16km$, and a terminal velocity of $1600m/s$.

Parameter bias and uncertainty are not considered in this simulation. Figure 6(a)

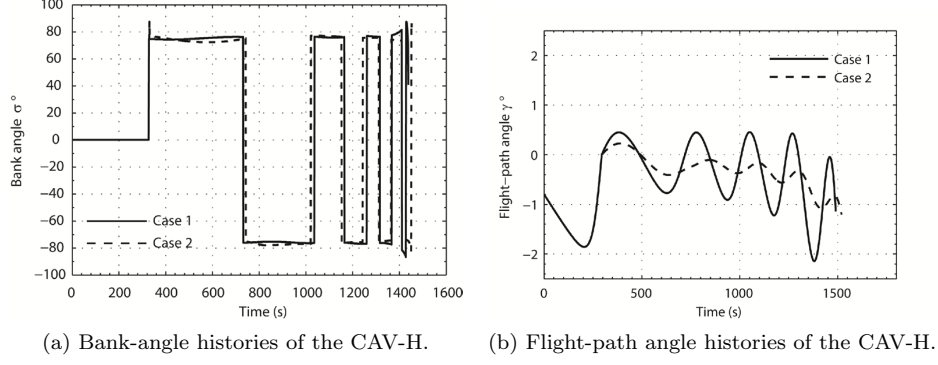(a) Curve of time-crossrange.    (b) Curve of longitude-latitude.

**Figure 7.** Trajectory characteristic in lateral plane.

indicates the typical trajectory characteristics for the longitudinal plane. Upon comparing the two cases, there were no phugoid trajectory oscillations, and the velocity-altitude histories are relatively smooth in case 2. Therefore, the feedback control law based on the aerodynamic load is feasible in this study. Figure 6. (b) shows the trajectories for the velocity-altitude profile. During the reentry process, the trajectory of the CAV-H is always located inside the reentry corridor, thus satisfying the requirements of various path constraints. The altitude and velocity of the landing site were $16.18km$ and $1644.6m/s$ respectively, in case 1 and $16.17km$ and $1622.2m/s$, respectively, in case 2. The simulation results obtained by the two algorithms indicate that the deviation in altitude is less than $1.5km$, and the velocity deviation is less than $50m/s$. Thus, the analytical predictor-corrector guidance algorithm proposed in this paper has higher guiding accuracy.

Figure 7 indicates the lateral trajectory characteristics of the gliding reentry, and the CAV-H performed several lateral maneuvers and finally reached the target accurately. The lateral guidance law always restricts the lateral movement of the CAV-H to the interior of the lateral corridor. During the process of approaching the target, the lateral corridor converged as the range-to-go decreased, whereas the lateral guidance law constantly revised the deviation until there was convergence to the set target. In case 1, the latitude and longitude of the landing site were $(64.94°, 64.98°)$, and in case 2, they were $(64.99°, 64.99°)$. Meanwhile, the downrange deviations for the two cases were 6.67 km and 1.11 km, respectively. The deviations from the latitude and longitude calculated by these two algorithms were all less than $0.15°$, and the distance between the landing site and target site was less than 10 km, which satisfies the guidance precision requirement.

Figure 8 indicates the attitude motion characteristics of the CAV-H. The maneuver of the CAV-H in the lateral corridor is achieved through the bank angle reversal logic. As the target was approaching, the lateral corridor gradually converged, and the frequency of the bank angle reversal increases (Figure8.a). The reversal times of the bank angle are related to $\Delta\psi_0$ . The greater $\Delta\psi_0$ is, the longer it takes the vehicle to arrive at the lateral boundary, which results in a reduction in the frequency of the bank angle reversal. However, the vehicle can not modify the crossrange in time when a larger $\Delta\psi_0$ is selected. As a result, the actual crossrange and flight time will increase, and the lateral guidance accuracy will be reduced. Comparing the two cases, the feedback control law only corrects the amplitude of the bank angle and does not increase the reversal frequency. Figure 8.(b) shows that the flight path angles $|\gamma|$ are less than 3 degrees in both cases, thus satisfying the assumption of a small flight path angle. The

13

(a) Bank-angle histories of the CAV-H.

(b) Flight-path angle histories of the CAV-H.

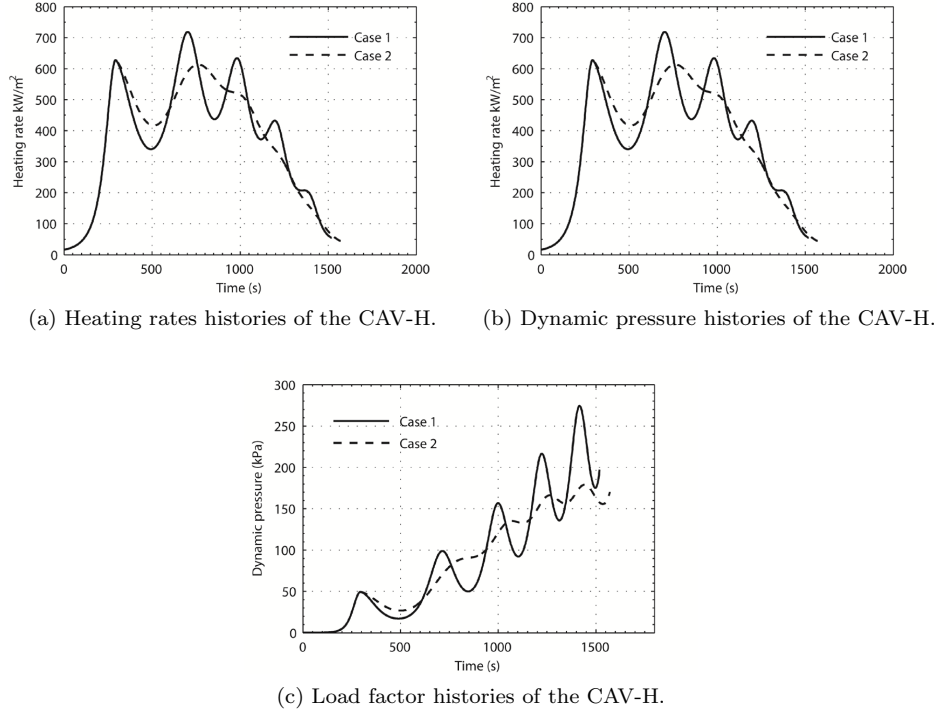**Figure 8.** Attitude motion characteristics of CAV-H.

deduced range-to-go Eq.(26) is suitable for the analytical predictor-corrector guidance algorithm.

The characteristic curves of all path constraints of the CAV-H during reentry gliding are given in Figure 9. In both cases, the heating rate, dynamic pressure and load factor constraints did not exceed the given maximum limits. Compared with case 1, the curve of the above path constraint in case 2 is smoother, and its oscillation amplitude is significantly reduced. The effect of heat/pressure protection is improved.
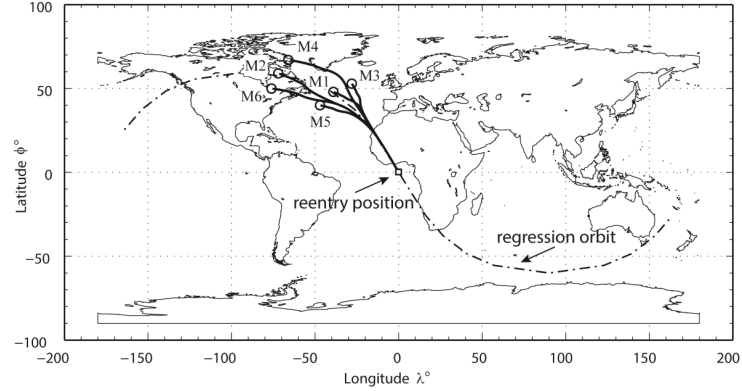
### 4.2. Entry missions

Next, we tested the performance of the proposed analytical predictor-corrector guidance algorithm. The assumption that the CAV-H follows the orbiter in a regression orbit with an inclination of $60°$, a regression period of 24 hours and an orbital period of 4 hours was used. The track of sub-satellite points is shown by the dotted line in Figure 10. To test the adaptability of the guidance algorithm for different downrange missions and to steer the vehicle in lateral maneuvers, 6 missions were arranged. They were divided into three groups. The first group ($M1$ and $M2$) is a small crossrange mission, and the target site is in the orbit plane of the initial reentry moment. The second group ($M3$ and $M4$) is on right side of the large crossrange mission, i.e., the target site is on the right side of the orbit plane (observed along the orbit running direction). The third group ($M5$ and $M6$) corresponds to the left side of the large crossrange mission. In each group, two missions were included, which were large and relatively small downrange. The initial downrange, crossrange, and terminal constraints for each mission are shown in Table 1.

Figure 10 illustrates the sub-satellite points formed by the CAV-H after the completion of all missions. Table 2 lists the terminal conditions that the guidance algorithm achieved for all missions (t for computing time). The test results indicate that the landing site for each mission (M1-M6) was not more than 15 km from the given target site, the velocity error was less than $100 m/s$, and the altitude error was less than 1 km. The guidance algorithm can adapt to the mission requirements of different longitudinal ranges. To accomplish reentry missions outside the orbit plane, the guidance algorithm also has the ability to steer the vehicle in lateral maneuvers. According to the calculation results of the M3-M6 missions, the CAV-H can accurately reach the target of 1000 km on both sides of the orbit plane, and the deviations in the longitude and latitude were less than $0.15°$. The guidance algorithm could make full use of

14

(a) Heating rates histories of the CAV-H.

(b) Dynamic pressure histories of the CAV-H.

(c) Load factor histories of the CAV-H.

**Figure 9.** Characteristic curve of path constraint.

CAV-H's high maneuver ability, significantly increasing its reentry coverage.



**Figure 10.** The track of sub-satellite points.

When the CAV-H was separated from the orbiter, the reentry position was chosen as the intersection of the equator and the meridian, i.e., the latitude and longitude coordinates were $(0°, 0°)$. The initial altitude was 120 km. The magnitude of the velocity was 7600 m/s and the direction along the tangent of the regression orbit at the reentry position. Thus, the initial azimuth angle was $30°$. Finally, the initial flight path angle was set to $-0.8°$. The path constraints of all of the missions were the same as those described in section 4.1. Considering the control capability of the vehicle, the flight control authority was restricted by a maximum bank angle of $85°$. The maximum bank

15

**Table 1.** Entry mission scenarios.

| Missions | Downrange[$s_{togo}$(km)] | Crossrange [$\chi_0$ (km)] | Velocity [$v_f$ (m/s)] | Altitude [$h_f$(km)] |
|----------|------------------|------------------|------------------|------------------|
| M1 | 6523.5 | -43.9 | 2500 | 16 |
| M2 | 8989.2 | 27.9 | 2300 | 16 |
| M3 | 6438.4 | -989.2 | 2500 | 16 |
| M4 | 8990.7 | -966.5 | 2300 | 16 |
| M5 | 6505.3 | -1048.3 | 2500 | 16 |
| M6 | 9012.8 | 1005.1 | 2300 | 16 |

**Table 2.** TAEM condition errors and computation times.

| Missions | $\Delta h_f$(m) | $\Delta v_f$(m/s) | $\Delta s_f$(km) | $\Delta\theta_f$(deg) | $\Delta\phi_f$(deg) | $t/s$ |
|----------|----------|----------|----------|----------|----------|------|
| M1 | 163.3 | 50.20 | 13.90 | 0.08 | 0.08 | 0.76 |
| M2 | 180.5 | 54.6 | 6.86 | 0.08 | 0.01 | 0.86 |
| M3 | 120.8 | 77.73 | 6.42 | 0.03 | 0.05 | 0.75 |
| M4 | 109.6 | 91.09 | 11.12 | 0.10 | 0.02 | 0.84 |
| M5 | 163.7 | 80.18 | 11.89 | 0.10 | 0.03 | 0.76 |
| M6 | 100.2 | 84.81 | 3.29 | 0.01 | 0.00 | 0.84 |

angle rate was $40°/s$, and the maximum attack angle rate was $20°/s$.

## 5. Monte Carlo Simulations

The traditional guidance accuracy assessment method evaluates the dispersion of the landing site, which requires many flight tests. However, due to the high cost of a flight test and to the various conditions of test field constraints, the number of flight tests is extremely limited. Thus, it is difficult to meet the needs of the accuracy assessment. At present, Monte Carlo simulations are usually used to estimate the guidance accuracy. To evaluate the accuracy of the analytical predictor-corrector guidance algorithm and verify its robustness, 1000 Monte Carlo simulations were conducted for various disturbances. The entry condition, aerodynamic coefficient, atmospheric density, and vehicle mass are all dispersed. The dispersion distribution and their $3-\sigma$ values for the Gaussian distribution and the minimum/maximum value for a uniform distribution are provided in Table 3.

Figure 11 indicates the simulation result and the landing site dispersion statistics under the condition of a disturbance. The results show that the reentry process does not deviate from the original glide trajectory and can meet the requirements of the guidance in the presence of errors and perturbations. Longitudinal guidance results show that the range for a terminal altitude deviation is 51 m  427 m, and the max-

**Table 3.** Statistics of dispersions used in the Monte Carlo simulations.

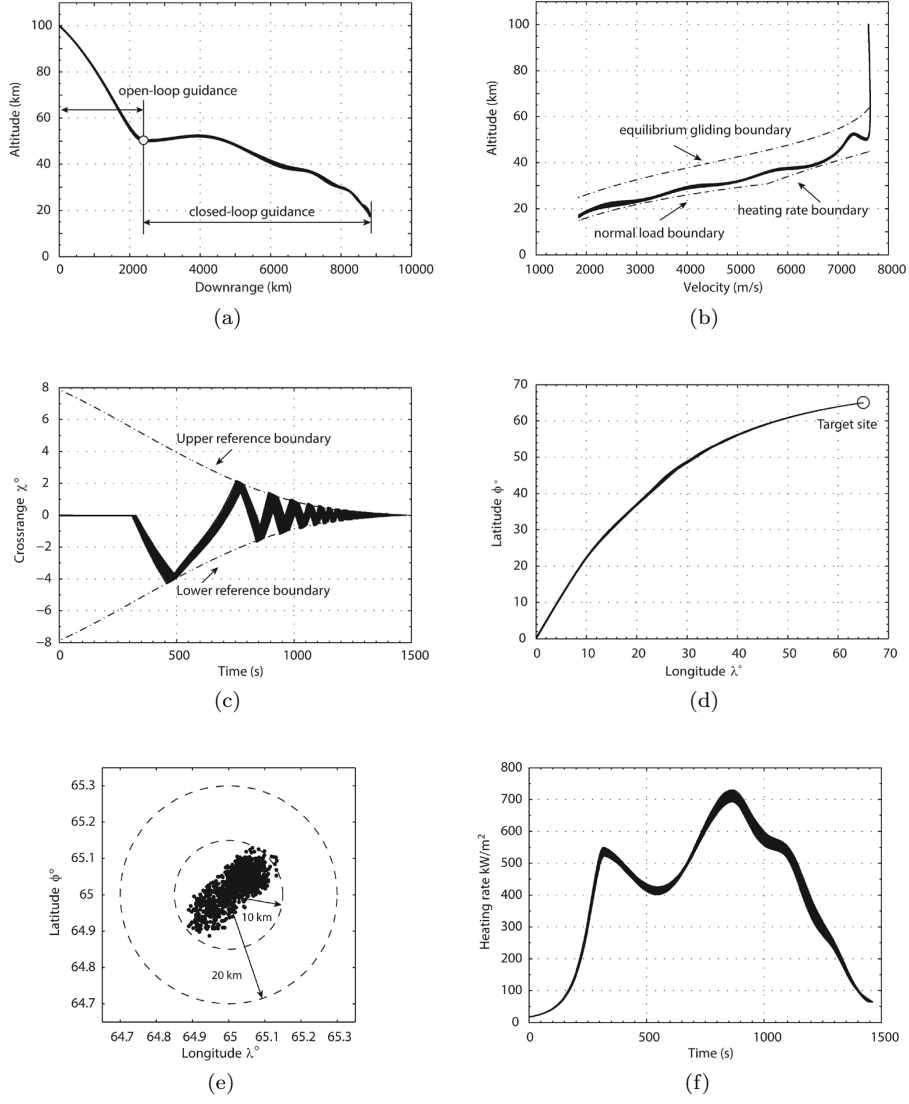| Parameters | Dispersion | $3-\sigma$ or min / max |
|----------|----------|----------|
| $\Delta\rho/(kg/m^3)$ | Uniform | $\pm15\%$ |
| $\Delta m/kg$ | Uniform | $\pm15\%$ |
| $\Delta C_L$ | Uniform | $\pm15\%$ |
| $\Delta C_D$ | Uniform | $\pm15\%$ |
| $\Delta h_0/km$ | Gaussian | $\pm300m$ |
| $\Delta\theta_0/(°)$ | Gaussian | $\pm0.15°$ |
| $\Delta\phi_0/(°)$ | Gaussian | $\pm0.15°$ |
| $\Delta v_0/ms^{-1}$ | Gaussian | $\pm100m/s$ |
| $\Delta\Gamma/(°)$ | Gaussian | $\pm0.15°$ |
| $\Delta\psi_0/(°)$ | Gaussian | $\pm0.15°$ |

(a)

(b)

(c)

(d)

(e)

(f)

**Figure 11.** Monte-Carlo simulation results.

imum deviation in the terminal velocity is 84m/s for the 1000 random interference trajectories, which meets the requirement of guidance precision (Figure 11.a-b). Under the action of a random disturbance, the velocity-altitude histories are smoother, and all can satisfy the path constraint. The trajectory of gliding is also relatively stable, and the feedback law of the bank angle can still remarkably restrain the periodic oscillation of the trajectory. Lateral guidance results show that all of the trajectory reversal rules are consistent (Figure 11(c)-(d)). The random perturbation does not change the lateral reversal rule; it only produces a small change in the reversal time. Therefore, the lateral guidance law is very robust. The landing sites are concentrated in the range of 10km from the target site (98.73%), the maximum range deviation is not more than 15 km (Figure 11.e), and the longitude and latitude deviations are less than 0.15°, which meet the accuracy requirements of the guidance to the landing site. Taking the heating rate as an example, all trajectories satisfy the maximum path constraint.

## 6. Conclusions

In this paper, an analytical predictor-corrector guidance method based on the feedback control of the bank angle was proposed. This guidance algorithm does not rely on a pre-designed reference trajectory; it can generate real-time guidance commands on request to control the vehicle to perform reentry missions. According to different reentry missions, the guidance algorithm can adjust the bank angle in time to meet the requirements of different downranges. For the reentry mission in the non-orbit plane, the guidance algorithm also has the ability to steer the vehicle in lateral maneuvers. The guidance algorithm can make full use of CAV-H's high maneuver ability, significantly increasing its reentry coverage. The feedback control law of the bank angle that we proposed can not only effectively eliminate the periodic oscillation of the glide trajectory but also reduce the amplitude of the heating rate, dynamic pressure and load factor. Therefore, the harsh environmental conditions of the vehicle during the reentry process are improved. Compared with the traditional numerical predictor-corrector guidance method, the calculation cost of this method is significantly reduced, and it exhibits higher guidance accuracy. Monte Carlo simulation results show that the proposed guidance method has good robustness, can adapt to changes in the mission and environment, and is very flexible and adaptable.

## References

[1] Walker S, Sherk J, Shell D, Schena R, Bergmann J, Gladbach J. The darpa/af falcon program: the hypersonic technology vehicle #2 (htv-2) flight demonstration phase. *15th AIAA International Space Planes and Hypersonic Systems and Technologies Conference*, 2008; 2539.

[2] Lu P. Entry guidance: a unified method. *Journal of Guidance Control and Dynamics* 2014; **37**(3):713–728.

[3] Wingrove RC. Survey of atmosphere re-entry guidance and control methods. *AIAA Journal* 1963; **1**(9):2019–2029.

[4] Saraf A, Leavitt J, Chen D, Mease K. Design and evaluation of an acceleration guidance algorithm for entry. *Journal of Spacecraft and Rockets* 2004; **41**(6):986–996.

[5] Dukeman G. Profile-following entry guidance using linear quadratic regulator theory. *AIAA guidance, navigation, and control conference and exhibit*, 2002; 4457.

[6] Li S, Lei H, Shao L, Xiao C. Multiple model tracking for hypersonic gliding vehicles with aerodynamic modeling and analysis. *IEEE Access* 2019; **7**:28 011–28 018.

[7] Anderson P, Schultz R, Stolarik E. A simple guidance scheme for lifting body reentry vehicles. *5th Aerospace Sciences Meeting*, 1967; 136.

[8] Kluever CA. Entry guidance using analytical atmospheric skip trajectories. *Journal of Guidance Control and Dynamics* 2008; **31**(5):1531–1535.

[9] Jianwei X, Jianzhong Q, Lei G, Wenhua C. Enhanced predictor–corrector mars entry guidance approach with atmospheric uncertainties. *IET Control Theory & Applications* 2019; .

[10] Ning G, Zhang S, Fang Z. Integrated entry guidance for reusable launch vehicle. *Chinese Journal of Aeronautics* 2007; **20**(1):1–8.

[11] Bharadwaj S, Anil, Rao V, Mease KD. Entry trajectory tracking law via feedback linearization. *Journal of Guidance Control and Dynamics* 2012; **21**(5):page. 726–732.

[12] Wang T, Zhang H, Tang G. Predictor-corrector guidance for entry vehicle based on fuzzy logic. *Proceedings of the Institution of Mechanical Engineers, Part G: Journal of Aerospace Engineering* 2019; **233**(2):472–482.

[13] Ping L. Predictor-corrector entry guidance for low-lifting vehicles. *Journal of Guidance Control and Dynamics* 2012; **31**(4):1067–1075.

[14] Xu ML, Chen KJ, Liu LH, Tang GJ. Quasi-equilibrium glide adaptive guidance for hypersonic vehicles. *Science China* 2012; **55**(3):856–866.

[15] Guang-Hua LI, Zhang HB, Tang GJ. Typical trajectory characteristics of hypersonic glide vehicle. *Journal of Astronautics* 2015; **36**(4):397–403.

[16] Shen Z, Ping L. Dynamic lateral entry guidance logic. *Journal of Guidance Control and Dynamics* 2012; **27**(6):949–959.